

# Isotopically selective collinear laser photoionization of accelerated helium atoms

Yu. A. Kudryavstev and V. V. Petrunin

*Institute of Spectroscopy, Academy of Sciences of the USSR*

(Submitted 21 July 1987)

Zh. Eksp. Teor. Fiz. **94**, 76–88 (April 1988)

Collinear two-step laser photoionization of  $^3\text{He}$  and  $^4\text{He}$  isotopes, accelerated to energies of up to 3.9 keV, is described. It is shown that the ionization selectivity in the case of the rare isotope  $^3\text{He}$  is  $10^6$  for a residual-gas pressure of  $10^{-7}$  Torr in the vacuum system. The sensitivity is limited by collisions that result in the excitation of fast metastable atoms to Rydberg states in the field-free region, and by impact ionization of fast atoms in the region of the ionizer. It is shown that the ionization of helium atoms excited to  $n^3D$  states occurs along the adiabatic and diabatic channels.

## 1. INTRODUCTION

The measurement of ultralow concentrations of rare isotopes is one of the unsolved problems in laser spectroscopy.<sup>1</sup> Laser detection of such isotopes is complicated by absorption in the wing of the spectral line due to the main isotope, which limits the attainable selectivity. A laser method of detecting rare isotopes, based on the stepwise, isotopically selective, excitation and ionization of atoms in an accelerated atomic beam, was proposed in Ref. 2. In this method, the magnitude of the artificially produced isotope shift

$$\frac{\Delta v^v}{v} = \frac{(2eU_A)^{1/2}}{c} \left( \frac{1}{M_1^{1/2}} - \frac{1}{M_2^{1/2}} \right)$$

exceeds the natural isotope shift<sup>2</sup> at 10 keV by a factor 10–100, where  $M_1$ ,  $M_2$  are the masses of the isotopes,  $c$  is the velocity of light, and  $eU_A$  is the kinetic energy of the atoms. In the case of collinear excitation, the absorption linewidth can be reduced down to the radiative width.<sup>3,4</sup> The first experiments<sup>5</sup> on two-step ionization of potassium isotopes, whose natural isotope shift is only 127 MHz, showed that  $^{40}\text{K}$  could be detected with a selectivity of  $10^5$  through isotopically selective excitation, but only in a one-step process, using pulsed dye lasers.

The next natural step toward a radical increase in detection selectivity could exploit multiplication of the excitation selectivities corresponding to the two steps, i.e.,  $S = S_1 S_2$  (Ref. 6). However, there are elementary physical processes that must first be investigated, and their influence on the ultimate selectivity elucidated. We have chosen the isotope  $^3\text{He}$ , whose natural concentration is  $1.4 \times 10^{-6}$  relative to the main isotope  $^4\text{He}$ , to investigate these processes. The isotope mass shift in the absorption spectrum of helium is relatively high and amounts to  $1.45 \text{ cm}^{-1}$  for the  $2^3S-3^3P$  transition<sup>7</sup> ( $\lambda = 3888 \text{ \AA}$ ). The shift rises to  $7.1 \text{ cm}^{-1}$  when a beam of helium atoms accelerated to 3.9 keV is excited. The isotope shift in the  $3^3P-n^3D$ ,  $n^3S$  transitions is  $3.15 \text{ cm}^{-1}$ . Under these conditions, one can readily produce two-step isotope selective excitation by using pulsed dye lasers with spectrum width of  $0.5 \text{ cm}^{-1}$ .

The maximum excitation selectivity in the case of the rare isotope, and laser radiation with a spectrum width  $\Delta v_l$  greater than the Doppler absorption linewidth, is given by

$$S = (\Delta v_{is} / \Gamma)^2 (2\Gamma / \Delta v_{is})$$

where  $\Gamma < \Delta v_{l1} \ll \Delta v_{is}$ ,  $\Gamma$  is the homogeneous absorption linewidth, and  $\Delta v_{is}$  is the isotope shift.

In the case of helium, the homogeneous absorption-line halfwidth for the above transition is governed by the lifetime of the  $3^3P$  state, and is  $\Gamma = 0.84 \text{ MHz}$ . The  $^3\text{He}$  excitation selectivity on the first and second excitation steps is  $7.2 \times 10^6$  and  $1.4 \times 10^6$ , respectively. The overall spectral sensitivity of two-step excitation is  $10^{13}$ .

Figure 1 shows the energy-level diagram of atomic helium. The ionization potential of helium is  $E_i = 24.6 \text{ eV}$ , so that stepwise ionization cannot be carried out from the ground state with existing lasers. However, it is possible to prepare fast neutral atoms in metastable states by using charge transfer between accelerated helium ions and alkali metal vapor. Potassium is a suitable candidate for this charge-transfer process (see Fig. 1). The electron binding energy in the  $2^1S$  and  $2^3S$  metastable states of helium is very close to the ionization energy of potassium in the  $4^2S$  ground state.

Helium atoms in the  $2^3S$  and  $2^1S$  metastable states are the main byproducts of the quasiresonant charge-transfer process between  $\text{He}^+$  and potassium. Helium atoms produced in the  $2^3P$  state undergo a transition after  $\tau = 98 \text{ ns}$  to

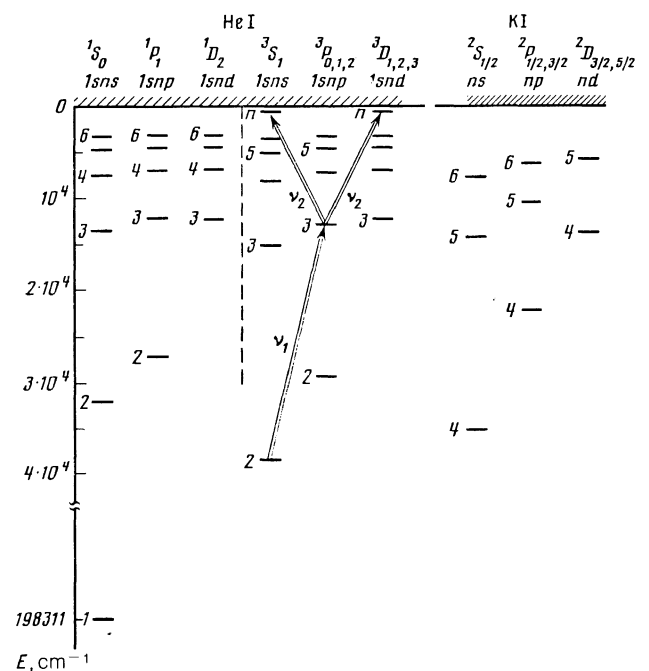


FIG. 1. Energy level diagram for helium and potassium atoms.

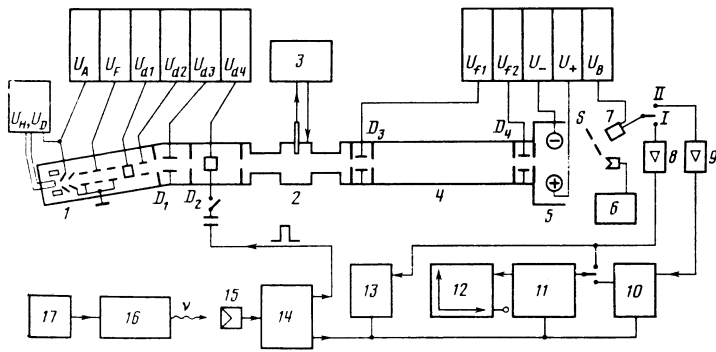


FIG. 2. Schematic diagram of the experimental setup: 1—ion source, 2—charge-transfer cell containing potassium vapor, 3—thermostat system, 4—field-free region, 5—field ionizers, 6—ion current monitor, 7—secondary-emission multiplier, 8, 9—preamplifier, 10—ion-counting gating system, 11—gating integrator, 12—X, Y recorder, 13—oscilloscope, 14—generator, 15—fast photocell, 16—excimer laser, 17—synchronization system,  $d_1, d_2, d_3, d_4$ —ion beam deflectors,  $D_1, D_2, D_3, D_4$ —diaphragms,  $f_1, f_2$ —filtering capacitors.

the long-lived  $2^3S$  state. At helium-ion energies of a few keV, three quarters of the atoms are formed in the metastable triplet state.<sup>8</sup> The charge-transfer cross section is  $1.2 \times 10^{-14} \text{ cm}^2$  (Ref. 9), which is much greater than the gas-kinetic collision cross section, so that the atomic beam has practically the same divergence after the charge-transfer cell as the original ion beam. Isotopically selective excitation of the accelerated helium atoms to the  $n^3S$  or  $n^3D$  Rydberg states, followed by ionization by the electric field, was accomplished from the  $2^3S$  metastable triplet state via the intermediate  $3^3P_{0,1,2}$  levels.

## 2. EXPERIMENTAL SETUP

A continuous beam of helium ions (Fig. 2) was produced by the hot-cathode gas-discharge source 1 in a nonuniform magnetic field. The ion energy (3.9 keV) was determined by the potential  $U_A$  of the shaping electrode relative to the grounded extracting electrode. The ion beam was then collimated by a single lens and was directed by deflectors  $d_1$  and  $d_2$  into the deflecting capacitor  $d_3$  which removed neutrals formed by resonant charge-transfers between  $\text{He}^+$  ions and helium atoms near the extracting electrode. After  $d_3$ , the beam of singly-charged ions entered the charge-transfer cell 2, filled with potassium vapor. Approximately 40% of the ions were transformed into neutral atoms when the hot part of the cell was 10 cm long and its temperature was  $160^\circ \text{C}$  (held constant to within  $\pm 0.5^\circ \text{C}$  by the thermostat 3). The filtering capacitor  $f_1$  removed ions still remaining in the beam. The field strength in this capacitor was 8 kV/cm, so that ions that could be excited during the charge-transfer process to Rydberg states with  $n > 17$  became ionized and were also extracted from the beam. The beam of metastable atoms then entered the field-free region 4 of length 100 cm. To reduce the residual-gas pressure, the field-free region was surrounded by a "jacket" held at liquid nitrogen temperature. In this region, the atoms were excited to Rydberg states by a laser beam containing frequencies  $\nu_1$  and  $\nu_2$ , and propagating antiparallel to the atomic beam. Ions produced in the field-free region as a result of collisions between fast atoms and residual-gas molecules could be extracted by the filtering capacitor  $f_2$ . Atoms prepared by the laser radiation in highly-excited states were ionized by the field ionizer 5 and were directed on to the detector 7 (secondary-electron multiplier). The ionizer consisted of two cylinders of radius  $r = 3 \text{ mm}$ , with centers separated by  $2H = 14 \text{ mm}$ . The ion detector could be set at  $20^\circ$  or  $45^\circ$  to the atomic-beam axis. Before they entered the detector, the ions passed through an adjustable slit  $s$  of width 0–6 mm. The beam diameter was

determined by the diameter of the diaphragm ( $D_4 = 2 \text{ mm}$ ). The ion-beam current was measured by a Faraday cup, and the effective atomic beam current by a secondary-emission detector. The effective neutral-atom current was 1–15 nA. The residual gas pressure in the vacuum system was about  $10^{-7} \text{ Torr}$ .

Figure 3 shows the time diagram of the operation of the system. The atomic-beam current measured by sensor 6 was modulated at 100 Hz (Fig. 3a) by the small ripple ( $\approx 0.2 \text{ V}$ ) on the discharge voltage across the ion source ( $U_D = 100 \text{ V}$ ). The excimer laser 16, used to pump the dye lasers, was fired at the instant of maximum current at a pulse repetition frequency of 16.7 Hz by the synchronizing unit 17. Part of the laser radiation was directed on the photocell 15 that triggered the generator 14. The latter produced sync pulses for the gating integrator 11, the ion counting system 10, and the oscilloscope 13.

The ion-signal detection system operated either in the integrating mode I or in the ion-counting mode II. The former was used for high signal strengths (in excess of 100 ions per pulse), and is shown in Fig. 3d. After the exposure of the atomic beam to the laser pulses and the preparation of the Rydberg atoms, the atoms at time  $t_0$  (Fig. 3b) travel towards the ionizer in which they are ionized and deflected onto the detector. The time  $t_1 - t_0$  is equal to the time-of-flight of the resulting ions between the ionizer and the secondary-emission multiplier. If the density of Rydberg atoms along the field-free region is constant, the signal rises linearly. The ions produced at the beginning of the field-free region (at  $D_3$ ) arrive at time  $t_4$ . The signal amplitude measured at this

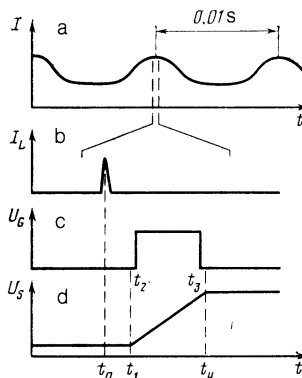


FIG. 3. Time-domain diagrams: a—ion (neutral) beam current, b—laser pulse, c—gating pulse for the ion counting system, d—ion signal in the integrating mode.

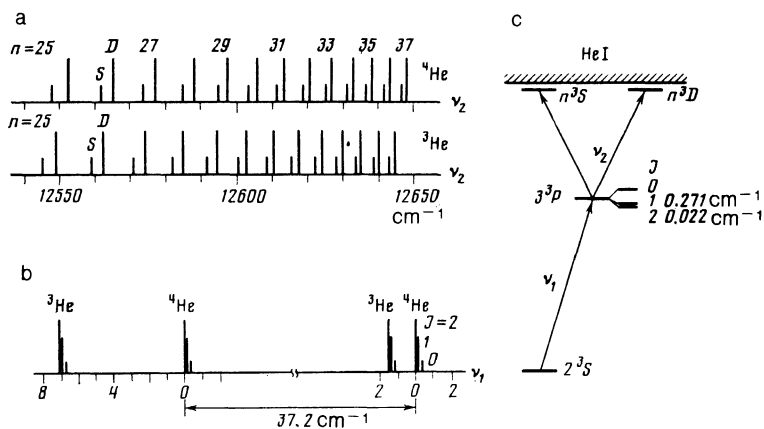


FIG. 4. Calculated absorption spectra of helium isotopes accelerated up to 3.9 keV: a—absorption spectra of  ${}^3\text{He}$  and  ${}^4\text{He}$  corresponding to the  $3^3P-n^3S, n^3D$  transitions, b—absorption spectrum of thermal and accelerated  ${}^3\text{He}$  and  ${}^4\text{He}$  atoms due to the  $2^3S-3^3P_{1,0,2}$  transitions, c—energy level diagram of He.

time is proportional to the number of recorded ions. The gating integrator, whose output is connected to an  $X$ - $Y$  plotter, measures and averages the signal at this time.

The ion-counting system was used to detect the rare isotope. This was dictated mostly by the fact that, as the laser frequencies are tuned to resonance with the rare isotope in the region of the filtering capacitors  $f_1, f_2$  and the ionizing capacitor, the Stark shift of high-lying levels always ensures that there is a region in which some of the atoms of the main isotope will also be in resonance with the laser frequency  $\nu_2$ . This background signal from the region of the filter  $f_2$  and the ionizer cannot be isolated by the ion-signal integrating system. This means that, to detect the  ${}^3\text{He}$  isotopes with concentrations less than  $10^{-3}$ , the single-ion signal was first amplified (9) and then entered the counting system 10 in which the pulses were counted only during the gate  $t_2-t_3$  (Fig. 3c). The amplitude of the signal produced in this way was proportional to the number of ions within the gate. The position and duration of the gate were chosen so that only ions from the field-free region were counted. The time resolution of the counting system was 10 ns. The signal from the counting system was also averaged and plotted by the  $X, Y$  recorder.

The mass composition of the ion beam was monitored by a time-of-flight method, for which a voltage  $U_{d4}$  was applied to the deflector  $d_4$ , and a 50 V "opening pulse" was produced by the generator 14 for  $\tau = 50$  ns. The measured impurity concentrations was less than 1% of the concentration of singly-charged helium ions.

The excitation of fast atoms to Rydberg states was produced by dye lasers pumped by the XeCl excimer laser ( $\lambda = 308$  nm). The laser for the second step was based on the generator-amplifier scheme. The width of the emission spectrum of both lasers was  $\Delta\nu_1 = 0.5$   $\text{cm}^{-1}$  and the pulse width at half height was 6 ns. The laser pulse of frequency  $\nu_2$  was delayed by 2 ns relative to the pulse for the first step. The wavelength of the laser for the second step was tunable in the range 780–810 nm. The laser frequencies could be scanned by external sawtooth voltage generators. Both laser beams were reflected by dielectric mirrors in the direction opposite to that of the atomic beam. The laser wavelength and linewidth were monitored by reflecting part of the radiation onto the slit of the MDR-4 monochromator and Fabry-Perot etalons. The plane of polarization of both laser beams was parallel to the electric field in the ionizing capacitor.

### 3. ISOTOPICALLY SELECTIVE IONIZATION OF HELIUM

Figure 4 shows the calculated spectra resulting from the two-step excitation of helium isotopes accelerated to 3.9 keV with the laser and atomic beams propagating in opposite directions. The natural isotope shift then adds to the artificially produced shift, and each line consists of three components because of the fine splitting of the intermediate  $3^3P$  level. The maximum separation between the components ( $0.271$   $\text{cm}^{-1}$ ) is less than the spectrum width  $\Delta\nu_1$  of the laser beams. The resonant frequency of the first transition in  ${}^4\text{He}$  is shifted toward the red by  $37.2$   $\text{cm}^{-1}$  as a result of acceleration (Fig. 4b); in  ${}^3\text{He}$ , it is shifted by  $42.85$   $\text{cm}^{-1}$  as compared with thermal atoms. The total isotope shift on the first step is  $7.1$   $\text{cm}^{-1}$ . Figure 4a shows the absorption spectra of accelerated  ${}^4\text{He}$  and  ${}^3\text{He}$  on the second step. These spectra can be used to select the frequency  $\nu_2$  for the selective excitation of the isotope  ${}^4\text{He}$ . Since the isotope shift is comparable with the separation between the  ${}^3S$  and  ${}^3D$  lines of the same isotope, the stronger  ${}^3D$  line of  ${}^3\text{He}$  may coincide with the  ${}^3S$  line of  ${}^4\text{He}$ .

Figure 5a shows the ionization spectrum when the first-step laser frequency  $\nu_1$  is in resonance with  ${}^4\text{He}$  ( $\nu_1 = 25671.4$   $\text{cm}^{-1}$ ). The ionization signal due to  ${}^3\text{He}$  with a relative concentration of  $10^{-4}$  is shown in Fig. 5b and was

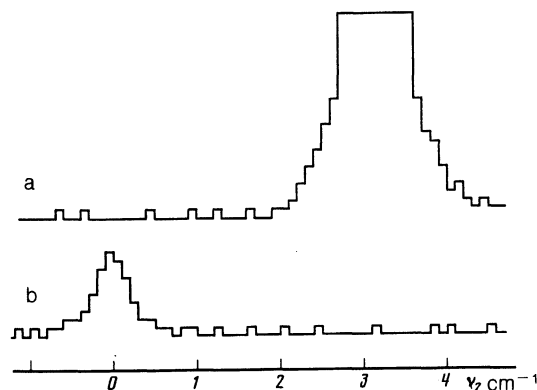


FIG. 5. Ion signal recorded by scanning the second-step  $\nu_2$  laser frequency ( $3^3P-2^3D$  transition): a—first-step frequency  $\nu_1 = 25671.4$   $\text{cm}^{-1}$  in resonance with  ${}^4\text{He}$ , b— $\nu_1 = 25664.3$   $\text{cm}^{-1}$  in resonance with  ${}^3\text{He}$ , [ ${}^3\text{He}$ ] =  $10^{-4}$ . Average over 16 pulses.

obtained for a  $7.1 \text{ cm}^{-1}$  shift of the frequency  $\nu_1$  toward the red. It is clear that, in this case, the  $^4\text{He}$  signal is totally absent, and the detection selectivity is  $10^6$ , and is limited by background ions. The reasons for the appearance of the background, and also the formation of ion signal, will be discussed later.

#### 4. IONIZATION OF RYDBERG ATOMS IN A TRANSVERSE ELECTRIC FIELD

Fast atoms excited to the  $n^3S$  and  $n^3D$  states were ionized by the transverse electric field of the ionizing capacitor (the electric field  $\mathbf{E}$  was perpendicular to the direction of motion of the atoms). The same field was used to deflect ions onto the adjustable slit  $s$  in front of the detector. Figure 6b shows the calculated electric field strength  $F_x$  on the axis of the atomic beam. In the beam section perpendicular to the  $Y$  axis, the field can be regarded as practically constant over the beam diameter of 2 mm.

In contrast to ions, Rydberg atoms entering the ionizing capacitor experience the deflecting electrical field only after they become ionized, and are deflected by a small angle. To ensure that these signal ions fall on the slit, the field must be increased relative to the field necessary to deflect ions produced before the ionizing capacitor. This means that the voltage across the ionizing capacitor, for which the signal due to ionization of atoms in highly excited states is observed after the slit, depends on the particular point (i.e., the particular field strength) at which the given state is ionized. At the same time, the field strength in which the Rydberg atoms become ionized depends significantly on the evolution of the atom in the growing electric field.

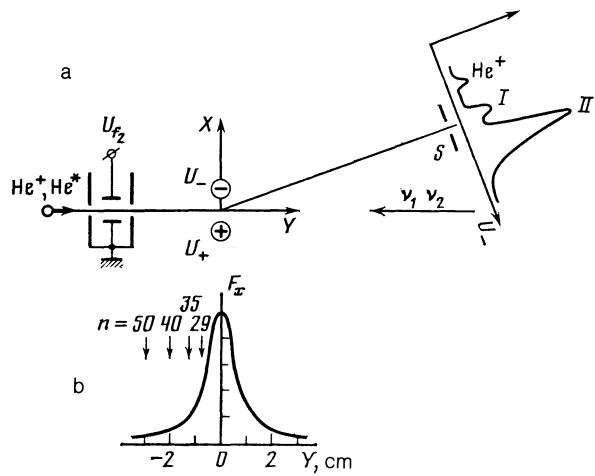


FIG. 6. (a) Disposition of the filtering ( $f_2$ ) and ionizing capacitors; (b) electric field strength on the axis of the ionizing capacitor. Arrows show the position of points at which atoms excited to different  $n^3S$  levels are ionized for  $U_{\pm} = \pm 1000 \text{ V}$ .

In a strong electric field,<sup>10</sup> the Stark effect is much greater than the fine splitting, and the energy level of the hydrogen atom with principal quantum number  $n$  and angular momentum component  $|m_1|$  splits into  $n - |m_1|$  Stark sublevels that experience the linear Stark effect (see Fig. 7). A hydrogen atom in the lowest ( $n_1 = 0$ ) Stark sublevel with  $|m_1| = 0$  is ionized by the electric field  $F_{\text{crit}} = 1/16n^4$ . Stronger fields are necessary for  $n_1 > 0$ . In contrast to the hydrogen atom, the presence of non-Coulomb terms in the Hamiltonian for the many-electron atom leads to the ap-

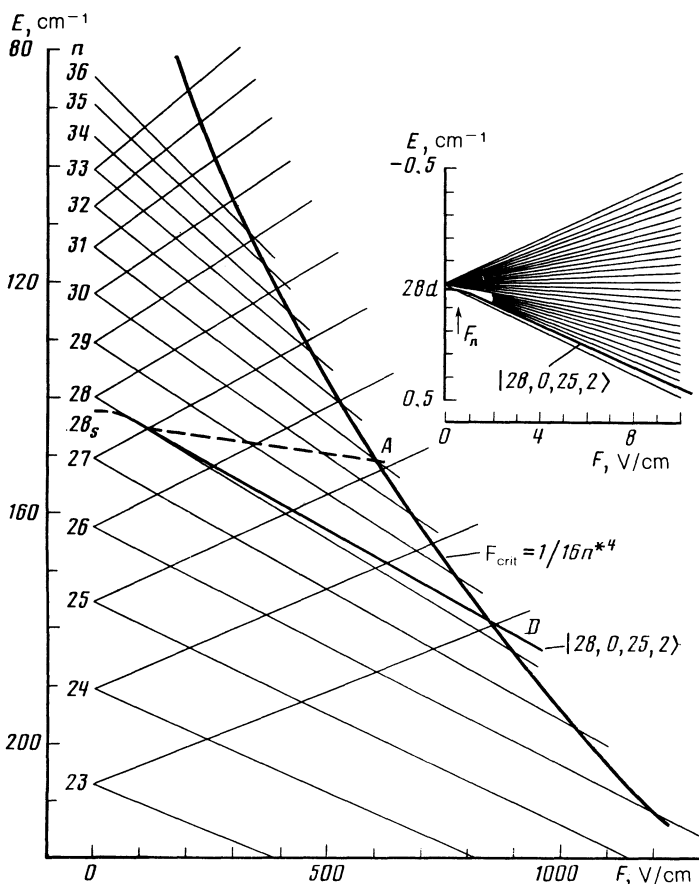


FIG. 7. Diagram showing the hydrogen-like Stark states with  $m_1 = 0$ . Only the extreme levels ( $m_1 = 0, n_2 = 0$ ) in the Stark set are shown for each  $n$ . The dashed line shows the adiabatic evolution toward the ionization limit of the  $28^3S$  and  $28^3D$  states with  $m_1 = 0$ . The straight line corresponds to the diabatic ionization of the  $28^3D$  states with  $|m_1| = 0$ . The insert shows the splitting of the Stark sublevels. The arrow indicates the field strength experienced by the 3.9 keV helium atoms moving in the geomagnetic field.  $E_n = -Z^2/2n^2 + 3Fn(n_1 - n_2)/2Z, n = n_1 + n_2 + m_1 + 1$ .

pearance in the zero-region field of quantum defects for states for different  $l$ , and also to the appearance of a coupling between Stark sublevels with the same  $|m_l|$ , which is particularly well-defined in the strong field in the region where Stark sublevels of the hydrogen atom that correspond to different  $n$  cross. This coupling ensures that the Stark sublevels of a real atom are split and in contrast to the hydrogen atom, cannot cross. A region of level quasicrossing is formed. The width of the resulting energy gap depends on the extent to which the levels are coupled. The coupling strength falls very rapidly with increasing  $|m_l|$ , and decreases monotonically with increasing  $n$ . An atom will enter the level quasicrossing region adiabatically when the field increases sufficiently slowly, and the energy gap is large. This is represented by the dashed curve in Fig. 7. In the neighborhood of the point  $A$ , the atom occupies levels that correspond to the low-lying Stark sublevels of the  $n = 31$  hydrogen set, which rapidly decay and become ionized. When the field grows rapidly enough, and (or) the energy gap is very small, diabatic evolution via the quasicrossing region predominates, and the atom reaches the  $D$  diabatically, following the hydrogen Stark sublevel that begins to decay in the neighborhood of  $D$ . Experiment has revealed both the adiabatic and diabatic evolution of Rydberg helium atoms in an electric field.

Figure 8 shows the ion signal as a function of the potential  $U_-$  on the ionizing capacitor for atoms excited to different  $^3S$  and  $^3D$  states ( $U_{f2} = 0$ ,  $U_+ = +750$  V, and deflection angle  $\alpha = 20^\circ$ ). The energy of the laser pulse corresponding to the first step is greater by a factor of 10 than the energy necessary to saturate the  $2^3S - 3^3P$  transition, and the pulse energy at the frequency  $\nu_2$  is smaller by a factor of 50 than the energy necessary to saturate transitions to the Rydberg states. Under these conditions, the peak that appears on all the plots at  $U_- = -850$  V, due to two-step ionization of metastable atoms via the  $3^3P$  level in the field-free region, is comparable in intensity with peaks due to the

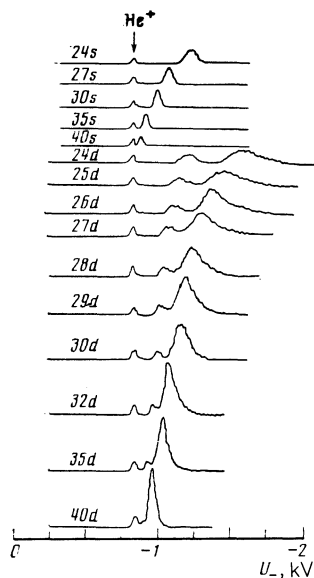


FIG. 8. Ion signal as function of the potential  $U_-$  on the ionizing capacitor when the laser beam is in resonance with different  $n^3S$  and  $n^3D$  levels.  $U_+ = 750$  V,  $\alpha = 20^\circ$ .

ionization of the Rydberg atoms. It is clear from the figure that this ionization system is dispersive in  $n$ .

The dependence of the ion signal on the voltage  $U_-$  during the excitation of the  $^3D$  states has two peaks that correspond to different electric-field intensities  $F$  for which ionization takes place. The signal corresponding to the excitation of  $^3S$  states has only one peak whose position is the same as that of the first peak of the  $^3D$  states with the same  $n$ . However, the width of the first peak due to the  $^3D$  states is somewhat greater than that for the  $^3S$  states and, under certain conditions, the former exhibits structure. We assume that the first peak (Fig. 8) is due to the adiabatic evolution and ionization of helium atoms with  $|m_l| = 0$  or 1, and the second peak corresponds mostly to the diabatic evolution in the field and to the ionization of atoms with  $|m_l| = 2$  (see Fig. 7). The  $^3S$  states can only have  $|m_l| = 0$ , and are ionized adiabatically. We note that the second peak due to the  $^3D$  states is wider than the first, and has a "tail" on the side of the larger values  $U_-$ . This can probably be explained by the presence of adiabatic transition to the upper Stark sublevels of hydrogen states with the lower  $n$ , which decay in stronger fields than the original sublevel.

The other possible reason for the broadening of the second peak may be laser excitation of several Stark sublevels when the electric field is applied. The insert in Fig. 7 shows the Stark level splitting in electric fields of a few V/cm. Since accelerated atoms ( $v = 4.3 \times 10^7$  cm/s) travel in the geomagnetic field  $\mathbf{B}$ , the laser excitation occurs in the effective field  $\mathbf{F} = \mathbf{v} \times \mathbf{B}$ . When  $B = 10^{-4}$  T, we have  $F = 0.43$  V/cm. The arrow in the insert of Fig. 7 shows the field strength for which the  $28^3D$  state is excited. As can be seen, the magnitude of the linear Stark effect for the  $n = 28$  sublevels is then of the order of the energy defect for the  $^3D$  state and, consequently, the selection rules for  $l$  can be partly lifted by the electric field. Several of the lower Stark sublevels can be excited at the same time when the laser spectrum width is  $\Delta\nu_l = 0.5$  cm $^{-1}$ .

The total number of ions detected in excited states with different principal quantum numbers  $n$  in the absence of saturation on the second excitation step should be proportional to  $n^{-3}$ . To ensure that the resultant signals due to different  $n$  are correctly compared, we must integrate the ion signal with respect to the angle  $\alpha$  at constant  $U_-$ . However, experimentally, it was easier to compare the integrated areas for different  $n$ , letting the horizontal axis in Fig. 8 represent  $U_- \partial\alpha/\partial U_-$  rather than  $U_-$ . The dependence on  $\partial\alpha/\partial U_-$  on  $U_-$  was determined from the broadening of the signal peaks with the slit wide open. The derivative  $\partial\alpha/\partial U_-$  varies smoothly by a factor of 1.4 in our interval of values  $U_-$ . Good agreement was observed for the resultant ion signal as a function of the level excitation number ( $2n^{-3}$ ) for  $n \geq 26$ .

We note that the ratio of signals corresponding to the first and second peaks (and hence the ratio of the number of atoms with different  $|m_l|$ ) was independent of the polarization of the laser radiation with frequencies  $\nu_1$  and  $\nu_2$ , and was probably determined by the evolution of the atom in the electric fields (including the Lorentz field due to the presence of the geomagnetic field and the installation itself) during its motion between the excitation region and the point at which it was ionized. The character of the evolution of the atom in weak fields, for which the magnitude of the Stark effect is comparable with fine splitting,<sup>11</sup> has a dominant effect on

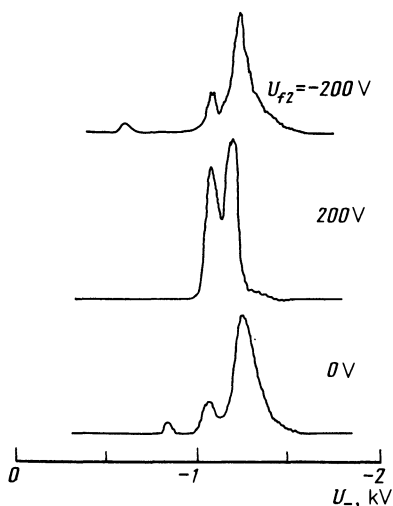


FIG. 9. Ion signal due to atoms excited to the  $28^3D$  state as a function of the potential  $U_-$  of the ionizing capacitor for different polarities of the filtering voltage.  $U_{f2}$ .  $U_+ = 750$  V,  $\alpha = 20^\circ$ .

the distribution over  $|m_l|$ . In the case of helium this corresponds to fields of less than 0.1 V/cm. For  $U_{f2}$  of positive polarity (Fig. 9), there is a point between the filtering and ionizing capacitors at which the electric field is zero. When excited atoms cross this region, there is a change in the population of states with  $|m_l| = 2$  and, hence the field strength in which the atom is ionized depends strongly on the character of the variation of this field.

### 5. $^3\text{He}$ DETECTION SENSITIVITY

We must now determine the maximum number of ions that can be detected per laser pulse. When the atomic beam current is  $I$ , number density of atoms in the beam is  $n_0 = I/vS$ , where  $v$  is the velocity of the atoms and  $S$  is the cross-sectional area of the atomic beam. After the charge-transfer cell, the fraction of atoms in the triplet state  $2^3S$  is  $\eta_{tr} = 0.75$ . The fraction of atoms undergoing transitions to the Rydberg state under the influence of the laser radiation is  $\eta_{exc}$ . When both transitions are saturated, we have  $\eta_{exc} = g_f/\Sigma g$ , where  $g_f$  is the degeneracy of the final state (equal to  $2l + 1$ ) and  $\Sigma g$  is the sum of the degeneracies of all the intermediate levels. The factor  $\eta_{exc}$  is equal to 1/9 or 5/9, depending on whether the  $^3S$  or the  $^3D$  state is excited. The next factor,  $g_i$ , represents the fact that, because of the finite lifetime  $\tau_n$  of the Rydberg atom as compared with the time necessary to cross the field-free region ( $\tau_c = L/v$ ), some of the atoms reaching the ionizer are not in the initial state  $n$ . The number of atoms reaching the field ionizer in the state  $n$  is

$$N = S \int_0^L n(x) dx = n_0 S L \frac{\tau_n}{\tau_c} \left[ 1 - \exp\left(-\frac{\tau_c}{\tau_n}\right) \right],$$

where  $n(x) = n_0 \exp(-x/v\tau_n)$ . The lifetime of the level with principal quantum number  $n$  is  $\tau_n = \alpha n^3$  (Ref. 12), where  $\alpha = 0.485$  ns for  $^3D$  states and 0.945 ns for  $n^3S$  states. When the length of the field-free region is 100 cm, and the  $n^3D$  levels are excited for  $n = 25-40$ , the value of the coefficient

$$\eta_i = (\tau_n/\tau_c) [1 - \exp(-\tau_c/\tau_n)]$$

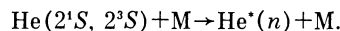
is found to be 0.86–0.96.

As shown in the last section, the ionization of atoms from different excited states occur in different electric fields, and this leads to a spread in the angle at which the ions are produced. The fraction of ions reaching the detector depends on the slit width  $s$ , which must be optimized for the signal-to-noise ratio. The independently measured efficiency  $\eta_D$  of the secondary-electron multiplier was 0.41. Thus, the total number of counts recorded during the time  $\tau_c$  taken by the atoms to cross the field-free region was

$$N_i = \eta_{tr} \eta_{exc} \eta_i \eta_s \eta_D I \frac{L}{v}.$$

When the effective current in the atomic beams is 1 nA, we find that  $N_i = 1.5 \times 10^3$  for the excitation of  $D$  levels and  $\eta_s = 0.7$ .

When the ionizing system is adjusted for the  $n \approx 30$  state, and the residual-gas pressure is  $10^{-7}$  Torr, the background for an effective atomic-beam current of 1 nA is  $10^{-3}$  counts per pulse. There are two basic reasons for the appearance of the background ions. First, when fast beam atoms collide with residual-gas molecules in the field-free space, they are excited to Rydberg states:



The resulting highly-excited atoms are no different from atoms produced selectively by the laser radiation, and are also ionized in the ionizer.

Second, fast atoms can be ionized in collisions with re-

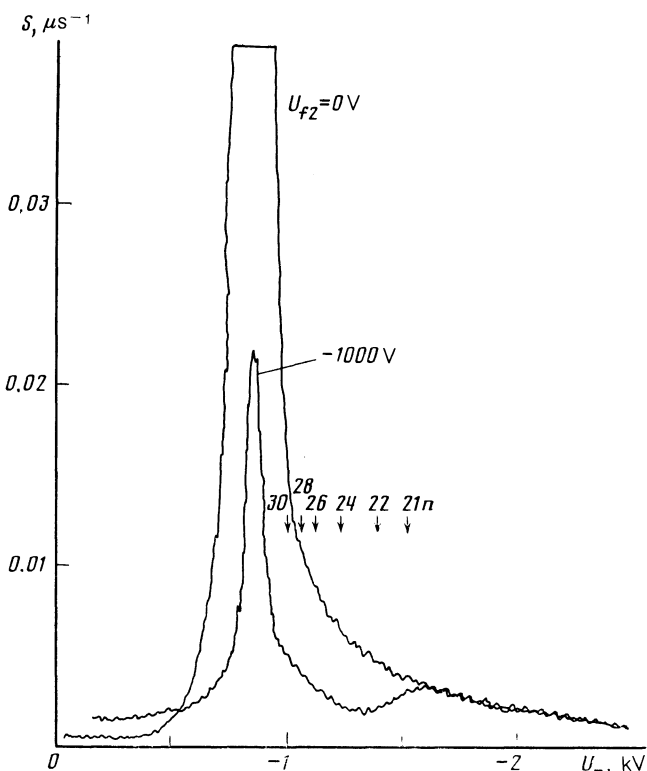
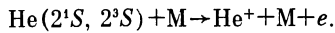


FIG. 10. Background signal as a function of the potential  $U_-$  of the ionizing capacitor for different values of the filtering voltage  $U_{f2}$ . Arrows indicate the position of peaks due to atoms excited to Rydberg states with principal quantum number  $n$  and  $l=0$ .  $U_+ = 750$  V,  $\alpha = 20^\circ$ ,  $P = 4 \times 10^{-7}$  Torr.

sidual-gas molecules in the region in which Rydberg atoms are field-ionized:



Ions produced in this region are also deflected on to the detector. The effect of these two processes on the background can be seen in Fig. 10. The arrows show the position of the signal peaks due to atoms excited to states with different  $n(l=0)$ . When the filtering voltage is  $U_{f2} = 0$ , the background from the  $n = 28$  neighborhood is due to the above two factors. For  $U_{f2} = 1000$  V, all the atoms produced in the field-free space with  $n > 24$  are ionized and are extracted from the beam. The remaining background signal is due to impact ionization of fast atoms in the region of the ionizer. It is clear that the contribution of these two processes to the background signal is roughly the same, even though the cross sections differ by factors of 500–1000.

Thus, the maximum selectivity, defined as the ratio of the number of counts due to Rydberg atoms produced by the laser radiation to the number of background counts is  $1.5 \times 10^6$  for the residual-gas pressure in the system of  $10^{-7}$  Torr. This estimate is confirmed by measurements of the ion signal due to  $^3\text{He}$  with relative concentration of  $10^{-4}$  (see Fig. 5).

## 6. CONCLUSION

Our results lead to the conclusion that two-step collinear photoionization of accelerated atoms can be a sensitive and an exceedingly selective method of analyzing the isotopic composition of matter. It provides a means of detecting  $^3\text{He}$  with a relative concentration of  $10^{-6}$  without resorting to additional mass-spectrometric techniques.

Field ionization of accelerated Rydberg atoms, prepared by laser radiation in particular quantum states, can be used to investigate the evolution of such atoms in electric fields and to study collisional processes involving the participation of highly-excited atoms.

<sup>1</sup>L. S. Letokhov, *Laser Photoionization Spectroscopy*, [in Russian] Nauka, Moscow, 1987 [English translation, Adam Hilger, London, 1988].

<sup>2</sup>Yu. A. Kudryavtsev, and V. S. Letokhov, *Appl. Phys. B* **29**, 219 (1982).

<sup>3</sup>S. L. Kaufman, *Opt. Comm.* **17**, 309 (1976).

<sup>4</sup>K. R. Anton, S. L. Kaufman, W. Klempt *et al.*, *Phys. Rev. Lett* **40**, 642 (1978).

<sup>5</sup>Yu. A. Kudryavtsev, V. S. Letokhov and V. V. Petrunin, *Pisma Zh. Eksp. Teor. Fiz.* **42**, 23 (1985) [*JETP Lett.* **42**, 26 (1985)].

<sup>6</sup>V. S. Letokhov and V. I. Mishin, *Opt. Comm.* **29** 168 (1979).

<sup>7</sup>A. A. Radtsig and B. M. Smirnov, *Reference Data on Atoms, Molecules, and Ions* (Springer, Berlin 1985), p. 98.

<sup>8</sup>C. Reynaud, Y. Pommier, V. N. Tuan, and M. Barat, *Phys. Rev. Lett.* **43**, 579 (1979).

<sup>9</sup>D. C. Lorents and J. R. Peterson, *Phys. Rev.* **182**, 152 (1969).

Translated by S. Chomet